Radiotherapy and Oncology 140 (2019) 110–115

Contents lists available at ScienceDirect

Radiotherapy and Oncology

journal homepage: www.thegreenjournal.com

Original Article

Reduced diffusion in normal appearing white matter of glioma patients following radio(chemo)therapy

F. Raschke [a,b,c,*], T. Wesemann [d], H. Wahl [d], S. Appold [b,e], M. Krause [a,b,c,e,f], J. Linn [d], E.G.C. Troost [a,b,c,e,f]

[a] Institute of Radiooncology – OncoRay, Helmholtz-Zentrum Dresden-Rossendorf, Rossendorf; [b] OncoRay – National Center for Radiation Research in Oncology, Faculty of Medicine and University Hospital Carl Gustav Carus, Technische Universität Dresden, Helmholtz-Zentrum Dresden – Rossendorf; [c] National Center for Tumor Diseases (NCT), Partner Site Dresden, Germany: German Cancer Research Center (DKFZ), Heidelberg, Germany; Faculty of Medicine and University Hospital Carl Gustav Carus, Technische Universität Dresden, Dresden, Germany, and; Helmholtz Association / Helmholtz-Zentrum Dresden -Rossendorf (HZDR), Dresden, Germany; [d] Institute of Neuroradiology, University Hospital Carl Gustav Carus and Medical Faculty of Technische Universität, Dresden; [e] Department of Radiotherapy and Radiation Oncology, Faculty of Medicine and University Hospital Carl Gustav Carus, Technische Universität Dresden; and [f] German Cancer Consortium (DKTK), Partner Site Dresden, and German Cancer Research Center (DKFZ), Heidelberg, Germany

ARTICLE INFO

Article history:
Received 2 April 2019
Received in revised form 4 June 2019
Accepted 14 June 2019
Available online 29 June 2019

Keywords:
White matter
Grey matter
Diffusion tensor imaging
Radiotherapy
Proton therapy
Photon therapy

ABSTRACT

Background and purpose: Standard treatment of high grade gliomas includes gross tumour resection followed by radio(chemo)therapy. Radiotherapy inevitably leads to irradiation of normal brain tissue. The goal of this prospective, longitudinal study was to use MRI to quantify normal appearing white and grey matter changes following radiation treatment as a function of dose and time after radiotherapy.

Materials and methods: Pre-radiotherapy (proton or photon therapy) MRI and follow-up MRIs collected in 3 monthly intervals thereafter were analysed for 22 glioma patients and included diffusion tensor imaging, quantitative T1, $T2^*$ and proton density mapping. Abnormal tissue was excluded from analysis. MR signal changes were quantified within different dose bin regions for grey and white matter and subsequently for whole brain white matter.

Results: We found significant reductions in mean diffusivity, radial diffusivity, axial diffusivity and $T2^*$ in normal appearing white matter regions receiving a radiation dose as low as 10–20 Gy within the observational period of up to 18 months. The magnitude of these changes increased with the received radiation dose and progressed with time after radiotherapy. Whole brain white matter also showed a significant reduction in radial diffusivity as a function of radiation dose and time after radiotherapy. No significant changes were observed in grey matter.

Conclusion: Diffusion tensor imaging and $T2^*$ imaging revealed normal appearing white matter changes following radiation treatment. The changes were dose dependant and progressed over time. Further work is needed to understand the underlying tissue changes and to correlate the observed diffusion changes with late brain malfunctions.

© 2019 Elsevier B.V. All rights reserved. Radiotherapy and Oncology 140 (2019) 110–115

Gliomas are the most common primary brain tumour in adults. Standard treatment of high grade gliomas includes gross tumour resection followed by radiotherapy with simultaneous or subsequent chemotherapy. The clinical target volume used for radiotherapy typically includes the resection cavity, the area of contrast enhancement seen on T1-weighted (T1w) MRI with an additional margin of 1–3 cm and T2-weighted (T2w) hyperintense areas to irradiate potential tumour infiltration [1,2]. Consequently, this leads to large irradiated volumes which inevitably include normal brain tissue. This can induce radiation related brain injuries which comprise anatomical changes, such as oedema, demyelination, gliosis and vascular abnormalities, as well as functional deficits, including short-term memory loss and cognitive impairment [3].

Irradiation with protons instead of photons reduces the radiation dose to surrounding brain in glioma patients [4]. To investigate if this reduction in radiation dose to normal appearing brain translates to measurable benefits for the patients, prospective clinical trials are ongoing, assessing the quality of life, neurocognitive

Abbreviations: T1w, T1-weighted; T2w, T2-weighted; AD, axial diffusivity; CT, computed tomography; CSF, cerebrospinal fluid; CTV, clinical target volume; DTI, diffusion tensor imaging; FA3, 3D gradient echo image with flip angle 3°; FA20, 3D gradient echo image with flip angle 20°; FA, fractional anisotropy; GM, grey matter; GTV, gross tumour volume; HC, healthy control; MD, mean diffusivity; PD, proton density; PTV, planning target volume; RD, radial diffusivity; RTx, radiotherapy; SDAM, saturated double angle method; TBV, termed tumour bed volume; WM, white matter.

* Corresponding author at: OncoRay, Medizinische Fakultät, PF41, Fetscherstr. 74, 01307 Dresden, Germany.
E-mail address: felix.raschke@oncoray.de (F. Raschke).

https://doi.org/10.1016/j.radonc.2019.06.022
0167-8140/© 2019 Elsevier B.V. All rights reserved.

functioning and MR image changes. In previous studies, radiation-induced normal tissue damage was assessed using oedema, haemorrhage or necrosis scored as binary events on T2w and contrast enhanced T1w MRI [5–7]. Drawbacks of these approaches are the loss of spatial information and low incidence rates [5,8], resulting in low predictive values. Additionally, there is a variable latency between irradiation and the occurrence of such severe side-effects. An early biomarker of late brain malfunctions or neurocognitive impairments would largely improve clinical trials and would enhance their capability to assess normal tissue complication rates in brain tumour radiotherapy.

Diffusion tensor imaging (DTI) allows probing of the tissue microstructure and therefore holds potential to detect earlier and less severe tissue changes not visible on conventional anatomical MRI. DTI has also proven to be a robust technique with low variability in a multicentre setting [9]. The most commonly used DTI parameters are fractional anisotropy (FA), mean diffusivity (MD), radial diffusivity (RD) and axial diffusivity (AD). Previous studies investigated primarily white matter (WM) diffusion changes following radiotherapy either within the whole brain [10,11] or focused on specific regions or tracts [12–19]. The most common diffusion results were a decrease in FA [10,12,14,15,19] and increased RD [10–12,14–16,19] consistent with demyelination [20,21], although deviations from this pattern were also reported [17,18].

Other relevant quantitative MR measures include T1, proton density (PD) and $T2^*$. T1 has shown to be a sensitive marker for myelin [22] and thus has the potential to support diffusion results related to demyelination or axonal loss. Similarly, quantitative PD mapping can be used to control for build-up or resolving of oedema, whereas $T2^*$ is used to assess tissue heterogeneity.

The aim of this longitudinal, prospective study was to quantify radiation-induced normal appearing brain changes as a function of radiation dose and time after radio(chemo)therapy. For this, we measured DTI as well as quantitative T1, PD and $T2^*$ changes within the normal appearing brain in a cohort of glioma patients. To minimise the impact of potential tumour progress on our analysis, we exclude all abnormal tissue across all time points from the analysis to solely focus on normal appearing white matter and grey matter (GM). Given the previously reported results, we hypothesised that FA and T1 decrease and RD increases in white matter, consistent with demyelination. We expected these changes to progress over time and to increase in magnitude with the received radiation dose.

Methods

Subjects

Data from glioma patients was taken from an ongoing, longitudinal study, which was approved by the local ethics committee [NCT02824731, EK22012016]. All patients underwent primary gross tumour resection followed by radio(chemo)therapy. Of 40 recruited patients, 27 patients had a pre-radiotherapy multimodal MRI and at least one identical follow-up MRI available. Follow-up scans were performed approximately 3 months after the end of radiotherapy and in 3-monthly intervals thereafter. Time points corresponding to histologically confirmed tumour progression were excluded, leaving data from 22 patients (age 47.8 y ± 13.9 y, range [28.9–76.7 y], 9 male) available for analysis. Clinical details and individual exclusion criteria for individual time points are listed in Supplementary Table 1.

Additionally, six healthy controls (HCs) (age 39.4 y ± 8.7 y, range [30.6–54.2 y], 4 male) underwent two multimodal MRI scans with an interval of 3.6 ± 0.5 months. This study was approved by the local ethics committee, and the participants gave written informed consent [DRKS-ID: DRKS00012600, EK267072017]. The healthy control MR data were collected in parallel to the patient data using the identical set-up described in the following section.

Data acquisition

All MRI data were acquired on a 3T Philips Ingenuity PET/MR scanner (Philips, Eindhoven, The Netherlands) using an 8 channel head coil.

DTI data were acquired with TR = 6500 ms, TE = 66 ms, FOV 224×224 mm^2, matrix size 112×112, slice thickness 2 mm, 60 slices, SENSE(AP) = 2, 32 diffusion directions at $b = 1000$ s/mm^2 and two $b = 0$ s/mm^2 volumes without diffusion gradients. Two additional $b = 0$ s/mm^2 volumes were acquired at identical parameters with opposite phase encoding direction.

3D FLAIR images were acquired in sagittal orientation with FOV 250×250 mm^2, acquisition matrix 252×249, reconstruction matrix 512×512, reconstructed slice thickness of 0.5 mm using overcontiguous slices, 360 slices, TR = 4800 ms, TE = 293 ms, TI = 1650 ms, 2 averages.

For T1 and PD mapping, two 3D gradient spoiled echo volumes were acquired in sagittal orientation with flip angles 3° (FA3) and 20° (FA20), TR = 10 ms, TE = 3.7 ms, FOV 224×224, matrix size 224×224, 1 mm slice thickness, 160 slices and Philips default RF-phase increment of 150°. For $T2^*$ mapping, axial 2D FFE images were acquired with TR = 1355 ms, TEs = 5.8/9.1/12.4/15.8/19.1 ms, FOV 256×256 mm^2, acquisition matrix 128×128, 47 slices with 2 mm thickness and 1 mm gap. A B1 map was acquired using the saturated double angle method (SDAM) [23] with flip angles 60° and 120°, TR = 734 ms, TE = 113 ms, FOV 224×224, matrix size 64×64, 4 mm slice thickness and 35 axial slices.

Radiation treatment planning

Computed tomography (CT) scans for radiation treatment planning were performed prior to radio(chemo)therapy with the patient positioned supine with an individual head support and mask. For radiation treatment planning, the CTs were co-registered with the pre- and post-surgery MRI scans (T1w, T2w, T1w with intravenous contrast agent) to define the tumour bed and potential residual tumour (termed tumour bed volume; TBV, or gross tumour volume; GTV, respectively). Depending on the tumour histology, the GTV/TBV was expanded by a 1–2 cm isotropic margin, corrected for anatomical boundaries, to derive the clinical target volume (CTV). For proton therapy, dose was prescribed to the CTV taking into account inherent proton range uncertainties, whereas for photon beam irradiation, a planning target volume (PTV) was computed expanding the CTV by an isotropic margin of 0.5 cm. For this analysis, the planning CTs, corresponding dose maps and CTV contours were retrieved from the planning workstation. CTV contours were converted to binary masks.

Data processing

In this study we focus on the analysis of normal appearing grey and white matter. Consequently, abnormality ROIs covering resection cavities and surrounding abnormal tissue were manually contoured on reconstructed axial FLAIR images with 4 mm slice thickness for each patient and each visit to exclude these areas from further analysis.

DTI data were processed with topup [24] implemented in FSL [25] to correct for geometric distortions caused by B0 inhomogeneities and FSL dtifit to estimate the diffusion tensor for each voxel. Subsequently, maps for FA, MD, AD, RD and q maps were calculated. The anisotropy measure q was previously proposed and unlike FA is not normalised by the root mean square diffusion [26].

$T2^*$ maps were calculated from the 2D FFE images on the scanner console, assuming a mono-exponential decay. Quantitative T1 and PD maps were calculated from the FA3 and FA20 images and using the B1 and $T2^*$ maps. The resulting T1 maps were segmented into GM, WM and CSF using SPM12 (Statistical Parametric Mapping: https://www.fil.ion.ucl.ac.uk/spm/) after manually excluding all abnormal tissue using the previously created abnormality ROIs. These GM and WM masks were transferred to DTI and $T2^*$ space via a rigid body registration using ANTs [27,28].

Detailed data processing steps are described in the Supplementary materials.

Data analysis

All analyses focused on normal appearing white matter and grey matter of the whole brain. Normal appearing brain was defined as being outside the CTV and the previously drawn abnormality ROI. To ensure exclusion of the same tissue areas across all relevant time points, a combined abnormality mask across all visits was created for each patient. This was done by warping each abnormality mask to MNI space via the T1w images and warping the combined masks back to the original T1w images using ANTs [27,28] (see Supplementary Fig. 1). The cerebellum and brain stem were excluded from all analyses due to varying spatial coverage by the MRI sequences. This was done by warping the MNI standard brain and a corresponding cerebrum mask to each T1w image of each patient and each visit (see Supplementary Fig. 4).

In the first analysis, whole brain MR signal changes were calculated within different dose regions across all time points. For this, dose maps were divided into seven dose bins: 0–3 Gy, 3–10 Gy, 10–20 Gy, 20–30 Gy, 30–40 Gy, 40–50 Gy, >50 Gy. Mean signal intensities were extracted from whole brain GM ($T2^*$, MD, T1, PD) and whole brain WM ($T2^*$, T1, PD, MD, FA, q, AD, RD) for each dose bin using a tissue probability threshold of 0.95. Only voxels outside the CTV and combined abnormality ROI were considered. Dose bin regions containing less than 100 voxels were excluded from the analysis. A relative signal change between follow-up and baseline values was calculated as $\Delta S[\%] = 100 \times (S_f - S_{base})/S_{base}$. The mean relative signal change was calculated across all patients and for each dose bin region, and reported in the results section. The HC data set served as a control cohort to reveal potential systematic errors. We therefore warped the dose maps, CTV masks and combined abnormality masks from 22 patients to each of the six HC data sets via MNI space using ANTs (see Supplementary Fig. 5A and 5B), resulting in a total of $6 \times 22 = 132$ permutations. Similar to the patient data, the mean relative signal change across all 132 permutations was calculated for all dose bin regions. Relative signal changes in both the patient data and HC control data were evaluated using paired *t*-tests. A Bonferroni correction factor for multiple comparisons of 12 (4 comparisons in GM and 8 comparisons in WM) was used, resulting in a significance threshold of 0.0042.

In a second analysis, we investigated the impact of both time after radiotherapy and mean dose on whole brain white matter $T2^*$ and RD changes. For this, the mean MR signal and mean radiation dose were determined across all normal appearing WM voxels. The relative signal change ΔS was calculated for $T2^*$ and RD and across all available time points. A mixed linear model with repeated measurements $\Delta S[\%] = b_0 + b_1 \times Dose[\mathrm{Gy}] + b_2 \times Time[\mathrm{months}]$ was used to assess the influence of both time and mean dose on whole white matter $T2^*$ and RD changes, respectively (SPSS, IBM Corp. Released 2017. IBM SPSS Statistics for Windows, Version 25.0. Armonk, NY: IBM Corp.).

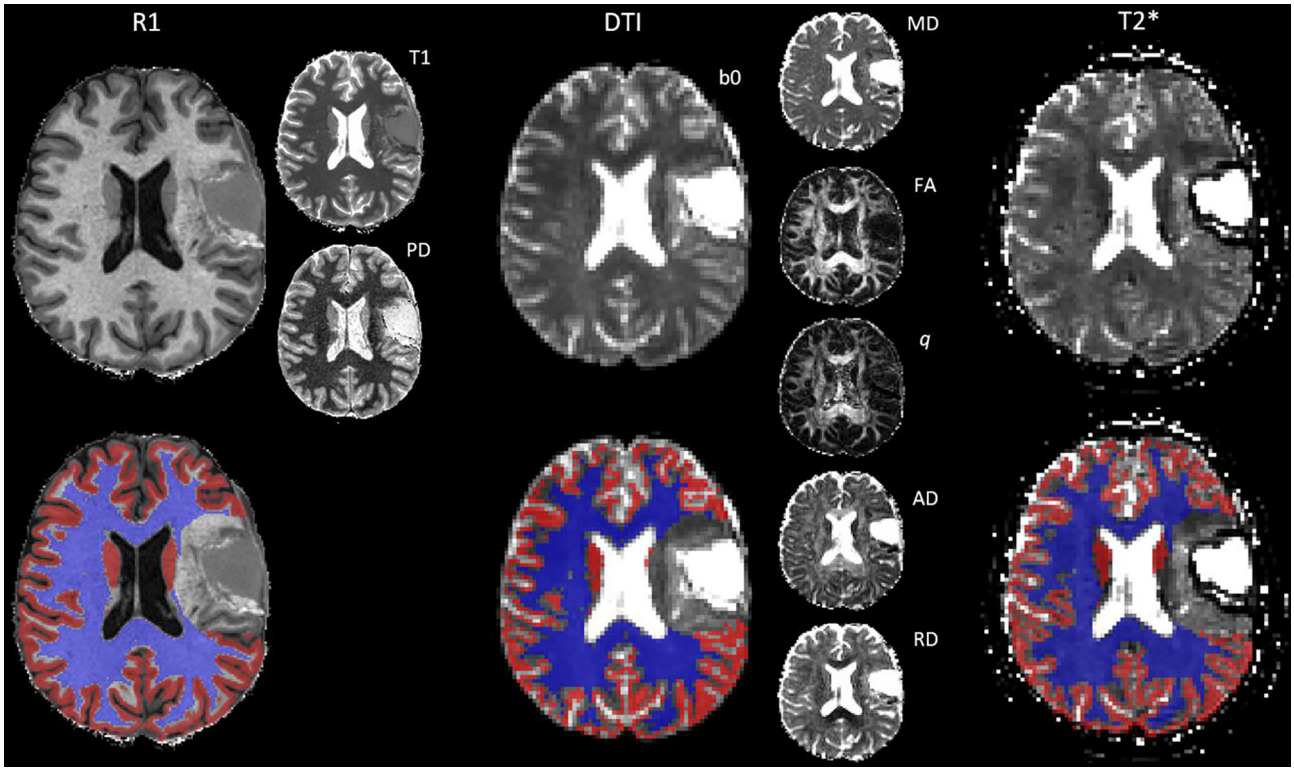

Fig. 1. Overview of the multiparametric MR images of a patient (#9) with a resected grade III anaplastic astrocytoma before the start of radiotherapy and adjuvant chemotherapy [PCV: consisting of procarbazine, lomustine (CCNU) and vincristine]. GM and WM masks were obtained by SPM12 segmentation of the T1 map. The GM (red) and WM masks (blue) were coregistered to the DTI b0 image and $T2^*$ map using a rigid body transformation and nearest neighbour interpolation. A subsequent probability threshold of 0.95 was chosen to binarise the GM and WM maps. Abnormal tissue was masked out prior to segmentation.

Results

Imaging data at 3, 6, 9, 12, 15 and 18 months after radio(chemo)therapy was available for $N = 19$, 15, 12, 11, 6 and 5 patients, respectively. Fig. 1 shows a complete set of quantitative axial images and corresponding grey matter and white matter masks for one patient.

Fig. 2 shows the mean relative MD, AD, RD, FA and T2* changes within the different dose bins in white matter. MD, AD, RD and T2* were significantly reduced both over time and dose, whereas the diffusion changes preceded T2* changes. FA showed a significant increase at high doses, whereas the anisotropy measure q showed no dose dependent changes (Supplementary Fig. 7). Nevertheless, there was a small, but significant reduction in q three months after radio(chemo)therapy, which normalised in the later time points. Neither T1 nor PD showed any significant changes (Supplementary Fig. 7). No significant changes were observed in grey matter (Supplementary Fig. 8). In the untreated control cohort, there were some systematic offsets smaller than 2% (see Fig. 2, Supplementary Figs. 7 and 8), however, no dose dependent changes were observed in either grey or white matter.

Following these results, we used a mixed linear model to investigate the influence of both time after radiotherapy and mean dose on whole brain white matter T2* and RD changes, respectively. We chose these two parameters, since they showed the largest magnitude of relative signal changes in the dose bin analysis. Mean dose

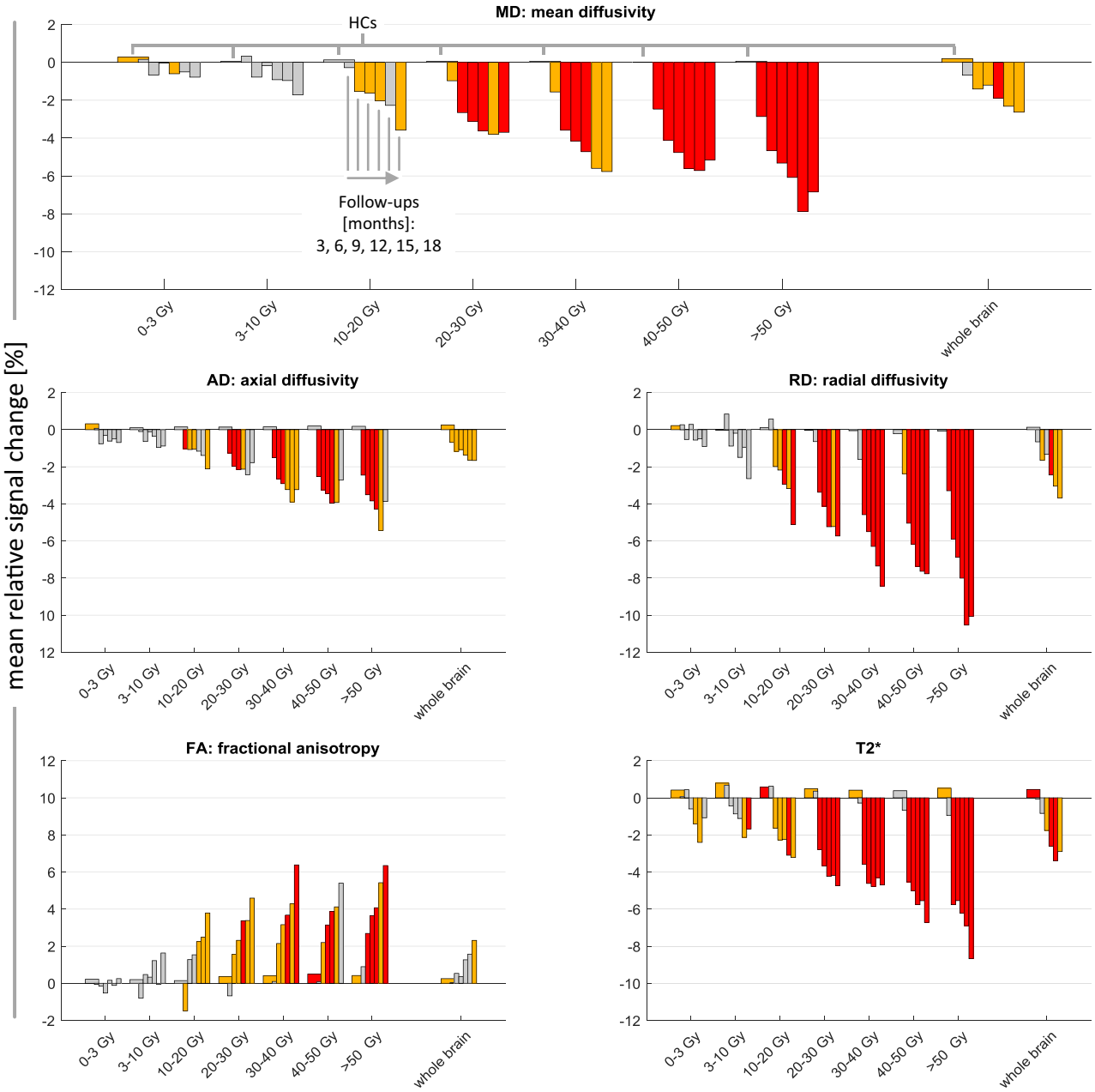

Fig. 2. Mean relative signal changes were calculated across all patients and all normal appearing cerebral white matter inside the seven dose bins. Whole brain corresponds to all of the normal appearing cerebral white matter from all dose regions. Mean relative signal changes are plotted for different time points after radio(chemo)therapy (see labels in the MD plot). Mean relative signal changes in the healthy controls (HC) are shown by wider bars. Grey bars indicate no significant signal change, orange bars correspond to $p < 0.05$ and red bars correspond to a Bonferroni corrected p-value of $p < 0.0042$. A version of this figure with error bars can be found in the supplementary material (Supplementary Fig. 6).

Table 1
Mixed linear models with repeated measurements were used to evaluate the relationship of both radiation dose and time after radiotherapy with the mean relative signal changes of radial diffusivity (RD) and $T2^*$ across whole brain white matter. Estimated parameters for the two mixed linear models $\Delta S[\%] = b_0 + b_1 \times Dose[Gy] + b_2 \times Time[months]$ for both RD and $T2^*$ are shown. An animation of the fitted RD model is provided as Supplementary material.

	Parameter	Estimate	Std.-error	T-stats	Significance
RD	b_0 (constant)	1.75	0.73	2.40	0.026
	b_1 (dose)	−0.15	0.04	−3.41	0.003
	b_2 (time)	−0.18	0.03	−7.09	<0.001
$T2^*$	b_0 (constant)	1.15	0.97	1.19	0.250
	b_1 (dose)	−0.13	0.06	−1.41	0.177
	b_2 (time)	−0.08	0.04	−3.26	0.002

in normal appearing white matter was 13.6 ± 9.7 Gy (protons: 9.6 ± 4.6 Gy, $N = 17$; photons 29.9 ± 10.2 Gy, $N = 4$; one patient with mixed treatment). The results of the linear mixed models for RD and $T2^*$ are shown in Table 1. RD significantly reduced with both mean dose and time at rates of −0.15% per Gy ($p = 0.003$) and −0.18% per month ($p < 0.001$), respectively. $T2^*$ changes were only significantly associated with time at −0.13% per month ($p = 0.002$), but not with the mean dose ($p = 0.177$). An animation of the mixed linear model fitted to the RD changes observed in white matter can be found in the Supplementary material.

Discussion

We hypothesised that, following radiation, FA would decrease and RD would increase with time and dose in normal appearing white matter thus mimicking typical diffusion observations associated with demyelination and axonal loss. Instead, we observed dose dependent and time progressive reductions in RD, MD, AD and $T2^*$. Additionally we have seen a trend of increasing FA, which is likely driven by the reduction in MD rather than a real anisotropy increase in the white matter. This is supported by the fact that the anisotropy measure q did not increase [26]. We therefore do not observe expected signs of axonal demyelination within our data, which is supported by stable T1 values, a sensitive marker for myelin [22]. Additionally, it has been shown that demyelinated white matter in mice shows significantly increased $T2^*$ [29], whereas we observe a significant $T2^*$ decrease.

The MD reduction in white matter following radiotherapy is mainly driven by a reduction in RD. A decrease in RD in white matter is usually associated with axonal swelling, as observed in acute and early phases of stroke [30]. However, in our study the RD decrease was in the order of 10%, compared to well over 50% in stroke and therefore not easily assessed visually.

Most previous studies investigating diffusion changes in white matter following radiotherapy found a decrease in FA and increase in MD and RD ranging from 2% to 50%, which is commonly interpreted as demyelination or axonal damage [10,12,14,16]. For AD, both increase [10–12] and decrease were previously reported [14,16,18]. Using tract-based spatial statistics (TBSS), Connor et al. [17] found patterns of FA decrease and RD and AD increase. However, they equally found white matter bundles with opposite behaviour, showing a significant AD and RD decrease. In a separate study, Zhu et al. [18] measured a significant decrease in AD and RD in white matter fibres after radiotherapy. Reactive astrogliosis, axonal degradation, axonal swelling and resolving oedema were previously suggested as possible explanations for decreasing RD and AD. Resolving oedema can be ruled out as a cause for reduced diffusivity observed in our study, as PD values show no significant changes. Astrogliosis is thought to be a response to cerebral injury but has shown to increase RD and reduce FA in white matter in mice, whereas an FA increase due to astrogliosis was only observed in grey matter [31]. Axonal degradation is a complex process, which includes axonal swelling, glial activation and axonal fragmentation [32]. Observing this process at different stages could explain the diverse diffusion results seen in different studies. Early stages with axonal swelling would cause a diffusion decrease as seen in our results whereas further progression including axonal demyelination is more likely to cause a diffusion increase, similar to the time course seen in stroke [30].

We also observed a significant decrease in $T2^*$, which could be caused by increased tissue heterogeneity. This can be an indicator for microglial activation caused by radiation [20,33] and could therefore also explain the reduction in overall diffusivity due to higher number of cell bodies in the white matter. However, we would then expect to see a simultaneous drop in anisotropy measures, which we did not observe. Additionally, the diffusion changes precede the $T2^*$ decrease, which might suggest a less direct relationship. The $T2^*$ reduction could also point towards changes in tissue oxygenation [34] and thus vascular alterations. This is supported by previously reported perfusion reductions observed in grey matter following radiotherapy [35] and would support the ischemia like behaviour of the diffusion metrics, albeit at a much smaller scale.

Future work is needed to connect the observations of this study to the underlying tissue changes. Specifically, we will analyse perfusion changes in white matter following radiotherapy to investigate vascular alterations. Similarly, glial cell density, neuronal health and neuro inflammation will be studied using MR spectroscopy [36]. Additionally, the observation period of the patients needs to be extended to investigate potential recovery of signal intensities and correlate the observed diffusion changes with late brain malfunctions. In a next step, we will investigate if occurrence of FLAIR hyperintensities can be predicted by diffusion reductions from previous time points.

For a more in-depth comparison of proton vs. photon based radiotherapy, a larger data set is needed. This includes investigating the effect of an equivalent proton and photon radiation dose on tissue. Nonetheless, we have shown that mean RD reduces significantly as a function of radiation dose across whole brain white matter. Consequently, these mean white matter changes are smaller in patients treated with protons compared to photons, since these patients typically receive a lower dose to the normal appearing brain.

Conclusion

We measured significant reductions in MD, AD, RD and $T2^*$ in white matter of glioma patients following radiotherapy. The magnitude of these changes progressed over time after radiotherapy and was greater in areas that received a higher radiation dose. The largest magnitude in change was observed for RD which also translated to significant time and dose dependant mean RD reductions across whole brain white matter. Further work is needed to understand the underlying tissue changes.

Declaration of Competing Interest

None.

Acknowledgements

We thank all patients and healthy volunteers for participating in the respective studies. We thank Prof F. A. Howe for the helpful discussions and both A. Dutz and Dr. S. Löck for advice on statistical analysis. This work was partly funded by the National Center for Tumor Diseases (NCT), Partner Site Dresden.

Appendix A. Supplementary data

Supplementary data to this article can be found online at https://doi.org/10.1016/j.radonc.2019.06.022.

References

[1] Brandes AA, Stupp R, Hau P, Lacombe D, Gorlia T, Tosoni A, et al. EORTC study 26041–22041: phase I/II study on concomitant and adjuvant temozolomide (TMZ) and radiotherapy (RT) with PTK787/ZK222584 (PTK/ZK) in newly diagnosed glioblastoma. Eur J Cancer 2010;46:348–54. https://doi.org/10.1016/j.ejca.2009.10.029. ISSN 1879-0852.

[2] Chang EL, Akyurek S, Avalos T, Rebueno N, Spicer C, Garcia J, et al. Evaluation of peritumoral edema in the delineation of radiotherapy clinical target volumes for glioblastoma. Int J Radiat Oncol Biol Phys 2007;68:144–50. https://doi.org/10.1016/j.ijrobp.2006.12.009.

[3] Greene-Schloesser D, Robbins ME. Radiation-induced cognitive impairment-from bench to bedside. Neuro-Oncology 2012;14(suppl 4):iv37–44. https://doi.org/10.1093/neuonc/nos196. ISSN 1523-5866.

[4] Eekers DBP, Roelofs E, Cubillos-Mesías M, Niël C, Smeenk RJ, Hoeben A, et al. Intensity-modulated proton therapy decreases dose to organs at risk in low-grade glioma patients: results of a multicentric in silico ROCOCO trial. Acta Oncol 2018:1–9. https://doi.org/10.1080/0284186X.2018.1529424. ISSN 1651-226X.

[5] Dutz A, Lühr A, Agolli L, Troost EGC, Krause M, Baumann M, et al. Development and validation of NTCP models for acute side-effects resulting from proton beam therapy of brain tumours. Radiother Oncol 2019;130:164–71. https://doi.org/10.1016/j.radonc.2018.06.036. ISSN 1879-0887.

[6] Gunther JR, Sato M, Chintagumpala M, Ketonen L, Jones JY, Allen PK, et al. Imaging changes in pediatric intracranial ependymoma patients treated with proton beam radiation therapy compared to intensity modulated radiation therapy. Int J Radiat Oncol Biol Phys 2015;93:54–63. https://doi.org/10.1016/j.ijrobp.2015.05.018. ISSN 1879-355X.

[7] Peeler CR, Mirkovic D, Titt U, Blanchard P, Gunther JR, Mahajan A, et al. Clinical evidence of variable proton biological effectiveness in pediatric patients treated for ependymoma. Radiother Oncol 2016;121:395–401. https://doi.org/10.1016/j.radonc.2016.11.001. ISSN 1879-0887.

[8] Lühr A, von Neubeck C, Krause M, Troost EGC. Relative biological effectiveness in proton beam therapy – Current knowledge and future challenges. Clin Transl Radiat Oncol 2018;9:35–41. https://doi.org/10.1016/j.ctro.2018.01.006. ISSN 2405-6308.

[9] Grech-Sollars M, Hales PW, Miyazaki K, Raschke F, Rodriguez D, Wilson M, et al. Multi-centre reproducibility of diffusion MRI parameters for clinical sequences in the brain: multi-centre reproducibility of diffusion MRI using clinical sequences. NMR Biomed 2015;28:468–85. https://doi.org/10.1002/nbm.3269. ISSN 1099-1492, URL http://dx.doi.org/10.1002/nbm.3269.

[10] Connor M, Karunamuni R, McDonald C, White N, Pettersson N, Moiseenko V, et al. Dose-dependent white matter damage after brain radiotherapy. Radiother Oncol 2016;121:209–16. https://doi.org/10.1016/j.radonc.2016.10.003. ISSN 1879-0887.

[11] Hope TR, Vardal J, Bjørnerud A, Larsson C, Arnesen MR, Salo RA, et al. Serial diffusion tensor imaging for early detection of radiation-induced injuries to normal-appearing white matter in high-grade glioma patients. J Magn Reson Imaging 2015;41:414–23. https://doi.org/10.1002/jmri.24533. http://dx.doi.org/10.1002/jmri.24533.

[12] Nagesh V, Tsien CI, Chenevert TL, Ross BD, Lawrence TS, Junick L, et al. Radiation-induced changes in normal-appearing white matter in patients with cerebral tumors: a diffusion tensor imaging study. Int J Radiat Oncol Biol Phys 2008;70:1002–10. https://doi.org/10.1016/j.ijrobp.2007.08.020. http://dx.doi.org/10.1016/j.ijrobp.2007.08.020.

[13] Chapman CH, Zhu T, Nazem-Zadeh M, Tao Y, Buchtel HA, Tsien CI, et al. Diffusion tensor imaging predicts cognitive function change following partial brain radiotherapy for low-grade and benign tumors. Radiother Oncol 2016;120:234–40. https://doi.org/10.1016/j.radonc.2016.06.021. ISSN 1879-0887.

[14] Chapman CH, Nazem-Zadeh M, Lee OE, Schipper MJ, Tsien CI, Lawrence TS, et al. Regional variation in brain white matter diffusion index changes following chemoradiotherapy: a prospective study using tract-based spatial statistics. PloS One 2013;8:e57768. https://doi.org/10.1371/journal.pone.0057768. ISSN 1932-6203.

[15] Nazem-Zadeh M-R, Chapman CH, Lawrence TL, Tsien CI, Cao Y. Radiation therapy effects on white matter fiber tracts of the limbic circuit: Radiation sensitivity of the limbic circuit fiber tracts. Med Phys 2012;39:5603–13. https://doi.org/10.1118/1.4745560. ISSN 0094-2405.

[16] Chapman CH, Nagesh V, Sundgren PC, Buchtel H, Chenevert TL, Junck L, et al. Diffusion tensor imaging of normal-appearing white matter as biomarker for radiation-induced late delayed cognitive decline. Int J Radiat Oncol Biol Phys 2012;82:2033–40. https://doi.org/10.1016/j.ijrobp.2011.01.068. ISSN 1879-355X.

[17] Connor M, Karunamuni R, McDonald C, Seibert T, White N, Moiseenko V, et al. Regional susceptibility to dose-dependent white matter damage after brain radiotherapy. Radiother Oncol 2017;123:209–17. https://doi.org/10.1016/j.radonc.2017.04.006. ISSN 1879-0887.

[18] Zhu T, Chapman CH, Tsien C, Kim M, Spratt DE, Lawrence TS, et al. Effect of the maximum dose on white matter fiber bundles using longitudinal diffusion tensor imaging. Int J Radiat Oncol Biol Phys 2016;96:696–705. https://doi.org/10.1016/j.ijrobp.2016.07.010. ISSN 1879-355X.

[19] Makola M, Douglas Ris M, Mahone EM, Yeates KO, Cecil KM. Long-term effects of radiation therapy on white matter of the corpus callosum: a diffusion tensor imaging study in children. Pediatr Radiol 2017;47:1809–16. https://doi.org/10.1007/s00247-017-3955-1. ISSN 1432-1998.

[20] Wang S, Wu EX, Qiu D, Leung LHT, Lau H-F, Khong P-L. Longitudinal diffusion tensor magnetic resonance imaging study of radiation-induced white matter damage in a rat model. Cancer Res 2009;69:1190–8. https://doi.org/10.1158/0008-5472.CAN-08-2661. ISSN 1538-7445.

[21] Jelescu IO, Zurek M, Winters KV, Veraart J, Rajaratnam A, Kim NS, et al. In vivo quantification of demyelination and recovery using compartment-specific diffusion MRI metrics validated by electron microscopy. NeuroImage 2016;132:104–14. https://doi.org/10.1016/j.neuroimage.2016.02.004. ISSN 1095-9572.

[22] Harkins KD, Xu J, Dula AN, Li K, Valentine WM, Gochberg DF, et al. The microstructural correlates of T1 in white matter. Magn Reson Med 2016;75:1341–5. https://doi.org/10.1002/mrm.25709. ISSN 1522-2594.

[23] Cunningham CH, Pauly JM, Nayak KS. Saturated double-angle method for rapid B1+ mapping. Magn Reson Med 2006;55:1326–33. https://doi.org/10.1002/mrm.20896. URL http://dx.doi.org/10.1002/mrm.20896.

[24] Andersson JLR, Skare S, Ashburner J. How to correct susceptibility distortions in spin-echo echo-planar images: application to diffusion tensor imaging. NeuroImage 2003;20:870–88. https://doi.org/10.1016/S1053-8119(03)00336-7. URL http://dx.doi.org/10.1016/S1053-8119(03)00336-7.

[25] Smith SM, Jenkinson M, Woolrich MW, Beckmann CF, Behrens TEJ, Johansen-Berg H, et al. Advances in functional and structural MR image analysis and implementation as FSL. NeuroImage 2004;23:S208–19. https://doi.org/10.1016/j.neuroimage.2004.07.051. ISSN 1053-8119.

[26] Peña A, Green HAL, Carpenter TA, Price SJ, Pickard JD, Gillard JH. Enhanced visualization and quantification of magnetic resonance diffusion tensor imaging using the p:q tensor decomposition. Br J Radiol 2006;79:101–9. https://doi.org/10.1259/bjr/24908512. http://dx.doi.org/10.1259/bjr/24908512.

[27] Avants BB, Tustison NJ, Song G, Cook PA, Klein A, Gee JC. A reproducible evaluation of ANTs similarity metric performance in brain image registration. NeuroImage 2011;54:2033–44. https://doi.org/10.1016/j.neuroimage.2010.09.025. ISSN 1095-9572.

[28] Tustison NJ, Avants BB. Explicit B-spline regularization in diffeomorphic image registration. Front Neuroinf 2013;7:39. https://doi.org/10.3389/fninf.2013.00039. ISSN 1662-5196.

[29] Lee J, Shmueli K, Kang B-T, Yao B, Fukunaga M, van Gelderen P, Palumbo S, Bosetti F, Silva AC, Duyn JH. The contribution of myelin to magnetic susceptibility-weighted contrasts in high-field MRI of the brain. NeuroImage 2012;59:3967–75. https://doi.org/10.1016/j.neuroimage.2011.10.076. ISSN 1095-9572.

[30] Fung SH, Roccatagliata L, Gonzalez RG, Schaefer PW. MR diffusion imaging in ischemic stroke. Neuroimag Clin N Am 2011;21:345–77. https://doi.org/10.1016/j.nic.2011.03.001. ISSN 1557-9867.

[31] Budde MD, Janes L, Gold E, Turtzo LC, Frank JA. The contribution of gliosis to diffusion tensor anisotropy and tractography following traumatic brain injury: validation in the rat using Fourier analysis of stained tissue sections. Brain 2011;134:2248–60. https://doi.org/10.1093/brain/awr161. ISSN 1460-2156.

[32] Saxena S, Caroni P. Mechanisms of axon degeneration: from development to disease. Prog Neurobiol 2007;83:174–91. https://doi.org/10.1016/j.pneurobio.2007.07.007. ISSN 0301-0082.

[33] Colton CA. Heterogeneity of microglial activation in the innate immune response in the brain. J Neuroimmune Pharmacol 2009;4:399–418. https://doi.org/10.1007/s11481-009-9164-4. ISSN 1557-1904.

[34] Hermier M, Nighoghossian N, Derex L, Wiart M, Nemoz C, Berthezene Y, Froment JC. Hypointense leptomeningeal vessels at T2*-weighted MRI in acute ischemic stroke. Neurology 2005;65:652–3. https://doi.org/10.1212/01.wnl.0000173036.95976.46. ISSN 1526-632X.

[35] Petr J, Platzek I, Seidlitz A, Mutsaerts HJMM, Hofheinz F, Schramm G, et al. Early and late effects of radiochemotherapy on cerebral blood flow in glioblastoma patients measured with non-invasive perfusion MRI. Radiother Oncol 2016;118:24–8. https://doi.org/10.1016/j.radonc.2015.12.017. http://dx.doi.org/10.1016/j.radonc.2015.12.017.

[36] Quarantelli Mario. MRI/MRS in neuroinflammation: methodology and applications. Clin Transl Imaging 2015;3:475–89. https://doi.org/10.1007/s40336-015-0142-y. ISSN 2281-5872.